Adsorption of atomic and molecular oxygen on the $LaMnO_3$(001) surface: *ab initio* supercell calculations and thermodynamics

Eugene A. Kotomin,*[ab] Yuri A. Mastrikov,[ab] Eugene Heifets[a] and Joachim Maier[a]

Received 14th March 2008, Accepted 12th May 2008
First published as an Advance Article on the web 20th June 2008
DOI: 10.1039/b804378g

We present and discuss the results of *ab initio* DFT plane-wave supercell calculations of the atomic and molecular oxygen adsorption and diffusion on the $LaMnO_3$ (001) surface which serves as a model material for a cathode of solid oxide fuel cells. The dissociative adsorption of O_2 molecules from the gas phase is energetically favorable on surface Mn ions even on a defect-free surface. The surface migration energy for adsorbed O ions is found to be quite high, 2.0 eV. We predict that the adsorbed O atoms could penetrate the electrode first plane when much more mobile surface oxygen vacancies (migration energy of 0.69 eV) approach the O ions strongly bound to the surface Mn ions. The formation of the O vacancy near the O atom adsorbed atop surface Mn ion leads to an increase of the O–Mn binding energy by 0.74 eV whereas the drop of this adsorbed O atom into a vacancy possesses no energy barrier. *Ab initio* thermodynamics predicts that at typical SOFC operation temperatures ($\sim$1200 K) the MnO_2 (001) surface with adsorbed O atoms is the most stable in a very wide range of oxygen gas pressures (above 10^{-2} atm).

Introduction

Optimization of materials for cathodes of solid oxide fuel cells (SOFC) is a scientifically challenging and technologically important problem.[1] A necessary prerequisite of systematic research is an understanding of the mechanism of oxygen reduction and, in particular, the identification of the rate determining steps.[2] Despite considerable experimental efforts, many fundamental questions remain open. It is in particular the surface diffusion step which is poorly understood and which is hard to tackle experimentally. At the moment, the most popular SOFC cathode material is Sr-doped $LaMnO_3$ (LSM). This material attracted recently considerable attention also due to its applications in spintronics and magnetic cooling[3] which stimulated several theoretical studies of magnetic properties of pure LSM surfaces.[4] Recently we performed a series of studies of the (100) and (110) $LaMnO_3$ (LMO) surfaces focused on atomic, electronic and magnetic structures (ref. 5 and references therein).

However, we are aware only of two literature reports that attempted to model an interaction of oxygen with LMO and LSM surfaces at the *ab initio* level.[6] In these calculations, a strongly polar (110) surface was chosen which consists of alternating planes $LaMnO/O_2/LaMnO/\ldots$ with opposite charges $+4e$, $-4e$, $+4e\ldots$ (per unit cell area). Moreover, the surface unit cell was very small and coincides with the bulk unit cell. This is why the performed modelling of the O_2 molecule on the LaMnO-terminated surface has in fact very little in common with molecular adsorption, but much more with the growth of a proper oxygen surface plane above the LaMnO plane, terminating the slab used. As is well known,[7] stabilization of such polar surfaces could be achieved by 50% reduction of the first plane charge due to self-consistent charge redistribution. That is, the O_2-terminated surface is expected to have instead of $-4e$ a charge of $-2e$ (per unit cell), which was exactly observed by the authors[6] for the dissociation products of a O_2 molecule.

In this paper, we model O adsorption on a much less polar LMO (001) surface consisting of alternating $MnO_2/LaO/\ldots$ planes with nominal charges $\pm 1e$, and use a large surface unit cell corresponding to 12.5% of the surface coverage by an adsorbate which corresponds to the SOFC operation conditions.[1] Oxygen reduction is a complex multi-step process. We focus here only on the first stage of the O interaction with the cathode surface which is the most probable rate-determining step.

We found the optimal sites for atomic and molecular adsorption, O_2 dissociation, and O atom surface diffusion. The final step of oxygen interaction with the SOFC cathode is the penetration of the adsorbed O atoms into the electrode where they encounter surface oxygen vacancies. This is why we also calculated the migration energy for surface and bulk oxygen vacancies. Since the SOFC operates at high temperatures, we complemented our DFT calculations by the thermodynamic analysis of the LMO surface stability at such temperatures. Due to electrical neutrality, the motion of the charged surface defect is accompanied by the motion of the surface electronic charge. As the latter does not significantly contributes to the activation energy, our results are transformable to SOFC fuel cell conditions in which the steady state electrodes are supplied from the outer circuit.

[a] *Max Planck Institute for Solid State Research, Heisenbergstr., 1, D-70569 Stuttgart, Germany. E-mail: sofia.weiglein@fkf.mpg.de; Fax: 49 711689 1722; Tel: 49 711689 1721*
[b] *Institute for Solid State Physics, University of Latvia, Kengaraga str. 8, Riga, LV-1063, Latvia. E-mail: kotomin@fkf.mpg.de; Fax: 371 7132 778; Tel: 371 7187 816*

Method

We employed *ab initio* DFT computer code VASP[8] with a plane wave basis set, PAW method to represent the atom cores and with the GGA-Perdew-Wang-91 exchange–correlation potential, employing the cut-off energy of 400 eV and 2×2×2 Monkhorst–Pack *k*-point mesh in the Brillouin zone.[9] Preliminary spin polarized calculations of the LMO bulk and the (001), (110) surfaces are in good agreement with experiment (when available).[5] In particular, for the experimental orthorhombic geometry the energetically most favourable is the A-type anti-ferromagnetic (AAF) configuration, in agreement with experiment, whereas the cubic lattice constant (stable above 750 K) exceeds only by 0.5% the experimental one. The calculated cohesive energy of 30.7 eV is close to the experimental value (31 eV). Calculations of the surface relaxation and surface energies show a weak dependence on the magnetic configuration.[5] Keeping in mind that the relevant effects (~0.1 eV ref. 5 and 6) are much smaller than the adsorption and migration energies under study (several eV) and that under operational SOFC conditions LMO is paramagnetic (T_N = 140 K), we performed all calculations for the ferromagnetic (FM) state with collinear spins. Moreover, the FM slab has the lowest energy. Neglect of spin polarisation results in considerable errors in material properties. We found in particular that 7- and 8-plane slabs are thick enough and show main property convergence.

For modelling oxygen adsorption based on our studies of pure surfaces,[5] we used here a 7-plane slab terminated on both sides with a MnO_2 plane covered by the adsorbate. Use of such symmetrical slab permits to avoid a problem of the surface dipole moment.[7] The periodically repeated slabs were separated by a vacuum gap of 15.8 Å (which corresponds to the thickness of an 8-plane slab). The chosen surface unit cell was the extended $2\sqrt{2} \times 2\sqrt{2}$ primitive unit cell, *i.e.* the surface coverage was 1/8 (12.5%).

Since our calculations correspond to 0 K, we used the relevant low-temperature *orthorhombic* unit cell with on-plane lattice constants a = 5.56 Å, b = 5.61 Å optimized for the bulk. All atomic coordinates were allowed to relax. Based on our experience for O adsorption on the $SrTiO_3$ (001) surface,[10] we studied oxygen adsorption over surface Mn, O ions and the hollow position (Fig. 1). The topological (Bader) effective atomic charges were calculated according to a method described in ref. 11. The same approach was applied to estimate atom magnetic moments. The oxygen atom adsorption energies $E_{ads}^{(at)}$ were calculated with respect to free oxygen atoms:

$$E_{ads}^{(at)}(O) = -\tfrac{1}{2}[E_{slab}^{(ads)}(O) - E_{slab} - 2E^{(O)}], \quad (1)$$

and with respect to free oxygen molecule:

$$E_{ads}^{(m)}(O) = -\tfrac{1}{2}[E_{slab}^{(ads)}(O) - E_{slab} - E^{(O2)}], \quad (2)$$

where $E_{slab}^{(ads)}$ is the total energy of a fully relaxed slab with two-sided adsorbate (O or O_2), E_{slab} is the same for a pure slab, $E^{(O)}$ is the energy of an isolated oxygen atom in the ground triplet state, and $E^{(O2)}$ is the total energy of isolated oxygen molecule in the triplet state. The prefactors 1/2 before brackets and 2 before $E^{(O)}$ appear since the interface is modelled by a substrate slab with two equivalent surfaces and both O_{ads} atoms and $(O_2)_{ads}$ molecule symmetrically positioned on both sides of the slab. The molecular adsorption energy was calculated in a similar way. The difference of $E_{ads}^{(at)}(O)$ and $E_{ads}^{(m)}(O)$ equals half the O_2 molecule binding energy.

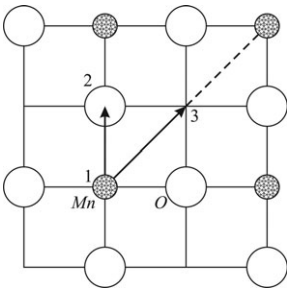

Fig. 1 Schematic top view of three possible oxygen adsorption sites on MnO_2 (001) surfaces: over Mn (1), O (2) and the hollow position (3). If O atom is adsorbed atop surface Mn, the possible saddle points of its migration could be position 2 or 3.

Results and discussion

Adsorption positions and energies

Table 1 shows a strong preference for O atom adsorption over the surface Mn ion, unlike the bridge position between Ti and O ions found for the isostructural $SrTiO_3$.[10] The difference is in line with the oxidizability of Mn^{3+} (compared to Ti^{4+}). Note that the top of the valence band in $LaMnO_3$ is largely due to Mn orbitals whereas the O orbitals generate the valence band top in $SrTiO_3$. The electron charge of 0.62 *e* is transferred to the adsorbed O atom from nearest surface ions (0.18 *e* from the nearest Mn, 0.16 *e* from the four nearest O ions and the rest 0.28 *e* from the next-nearest ions).

The analysis of the electron density redistribution (Fig. 2b) confirms that the O adsorption induces a quite local perturbation.

In the total density map (Fig. 2a) one can see very well the "wavy" atomic structure of the orthorhombic slab. As a result of O adsorption, the spin momentum of the Mn ion is strongly reduced. The test calculations performed for the high-temperature *cubic* phase (T > 750 K) give qualitatively similar results. In particular, the adsorption energy atop the Mn ion is 4.14 eV, ~3% larger than in the orthorhombic phase.

In order to check how the use of a nonstoichiometric slab affects the adsorption energy, we repeated the calculations for the stoichiometric cubic 8-plane slab. The O adsorption energy atop the Mn_s ion increased by 0.25 eV, or 6%. The adsorbed O charge practically does not change (−0.64 and −0.61 *e*, respectively) whereas the Mn ion charges exceed those on the perfect surface by 0.21 and 0.1 *e* for 7- and 8-plane slabs, respectively. The atomic charges on 7-plane cubic and orthorhombic surfaces are very close.

The adsorption position near the surface O_s ion is shown in Fig. 3a. This is practically identical to the *bridge position* found to be energetically most favourable for the $SrTiO_3$ (001) surface.[10] For $LaMnO_3$, this configuration turns out to be energetically less favourable, and the position above the hollow point, the most unfavourable. In these two cases the adsorbed O atom receives 0.3–0.5 *e* from the nearest surface

Table 1 Calculated adsorption properties for O atoms on MnO_2 (001) orthorhombic surface. Energies in eV, distances from the nearest ions, in Å, spins in μ_B. S, T stand for singlet and triplet. The effective atomic charges on a pure surface: 1.67 *e* (Mn), −1.17 *e* (O). 2×, 4× indicate a number of equivalent atoms

			Distance from O_{ads}		Charges			Spin	
Site	$E_{ads}^{(at)}$(O)	$E_{ads}^{(m)}$(O)	O_s	Mn_s	O_s	Mn_s	O_{ads}	Mn	O
Mn	4.02	1.07	2.55(4×)	1.63	−1.13	1.85	−0.62	2.20	S
O (bridge)	2.41	−0.54	1.50[a]	1.87 (2x)	−0.71	1.65	−0.48	3.61	S
Hollow	0.59	−2.36	3.28(2×)	—	−1.16 (4×)	—	−0.32	—	T
			3.18(2×)	—					

[a] The O–O dumbbell has an angle of 50° with the normal to the surface.

ions. Keeping in mind that the effective charges in LMO bulk and on the surface are considerably reduced due to the covalent component in the Mn–O chemical bonding as compared to the nominal charges (ref. 5 and heading in Table 1), the configuration above the O ion could be treated as formation of a kind of $O_2^{(2-)}$ peroxo-molecule[6] tilted by 50° towards the nearest Mn ion (Fig. 2).

The calculated adsorption energies with respect to an O atom in a free molecule, E_{ads}^{m}, eqn (2), are collected in Table 1. The positive value is obtained only for the O atom atop the Mn ion, where the energy gain due to adsorption of two O atoms is larger than the molecule dissociation energy. (Despite the fact that our calculations overestimate the dissociation energy of a O_2 molecule—5.9 eV *vs.* experimental 5.12 eV[12]—this does not affect our conclusion.)

Molecular adsorption

Along with the O atom adsorption, we calculated also the O_2 *molecular* adsorption over the energetically most favourable position atop the Mn ion in the two configurations: perpendicular and parallel to the surface (called hereafter *tilted* and *horizontal* in Table 2). The molecule binding energy is larger for the tilted adsorption (Table 2). The total charge of the adsorbed molecule is −0.42 *e* and the bond length 1.36 Å. (The bond length, 1.3 Å, of a free O_2 molecule calculated for the cut-off energy and other parameters used in this study is slightly larger than the experimental value of 1.21 Å[12]). The adsorbed molecule could be considered as a kind of superoxo-radical O_2^-.[6]

In the horizontal configuration the total charge of the molecule is larger, −0.65 *e*, the bond length increases up to 1.42 Å and is closer to the peroxo-radical O_2^{2-}. In both cases we observe chemisorption (unlike a weak physical adsorption of O_2 on $SrTiO_3$ (001) surface). A comparison of atomic and molecular adsorption energies (Tables 1 and 2), indicates that $2E_{ads}^{(m)}(O) > E_{ads}^{(m)}(O_2)$ for the most favourable adsorption site atop the Mn ion. This means that the *dissociative* molecular adsorption is favourable even on the defectless surface—in contrast to $SrTiO_3$.[10]

Defect migration

In calculations of defect migration paths and barrier energies we used the nudged elastic band method.[13,14] First of all, we simulated the adsorbed O atom migration from the energetically most favourable position atop a surface Mn_s ion along the (100) direction to the tilted O–O position (Fig. 3) and then this dumbbell rotation in the Mn–O–Mn plane towards the next Mn ion. The first step shows a monotonous increase by 1.6 eV whereas the second step costs an additional 0.4 eV. Thus, the overall barrier for the adsorbed O atom migration turns out to be 2.0 eV.

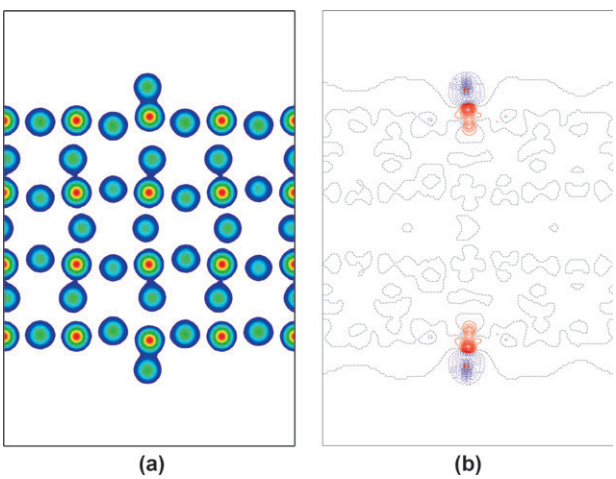

Fig. 2 The total (a) and difference (b) electron density maps for O atoms adsorbed over surface Mn ions on both sides of the symmetrical 7-plane slab. Red and blue colors indicate the electron density excess and deficiency, respectively. The density increment is 0.04 e $Å^{-3}$, black dash–dot line is a zero level.

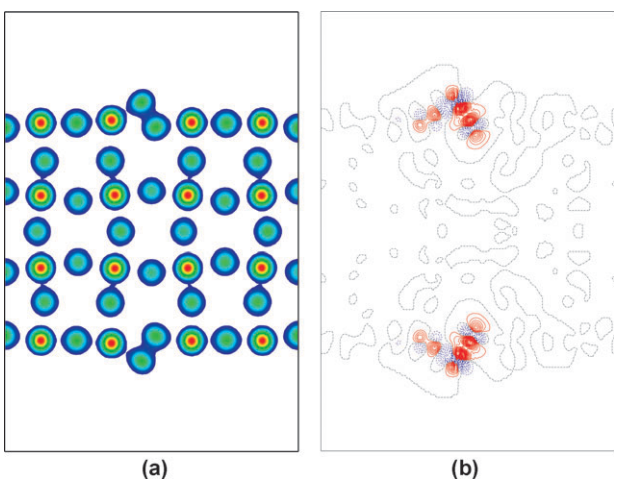

Fig. 3 As in Fig. 2 for O atom adsorbed at the bridge position near the surface O ion.

Table 2 Calculated adsorption properties for O_2 molecules on MnO_2 surface. Notations as in Table 1

		Distances		Charges[b]			Spin	
Oriented	$E_{ads}^{(m)}(O_2)$	O–O bond	O–Mn_s	O(1)	O(2)	Mn_s	Mn[c]	O_2
Tilted	1.13	1.36	1.86[a]	−0.29[a]	−0.13	1.78	3.12	D
Horizontal	0.89	1.42	1.85 1.90	−0.35	−0.30	1.77	3.05	S

[a] For O atom nearest to the surface. [b] Atoms in O_2 molecule. [c] 3.80 μ_B on a pure surface.

Following our $SrTiO_3$ studies,[15,16] we calculated also the equilibrium and barrier geometry for oxygen vacancies in the bulk and on the MnO_2 terminated surface. In the latter case, two pairs of the nearest Mn and La ions are strongly displaced from the vacancy (*ca.* 0.2 Å) whereas the two O ions—towards the vacancy (0.32 Å). The negative charge of the missing O ions is spread over the nearest ions, mostly Mn. The calculated vacancy migration energy is 0.67 eV, smaller than that calculated for the bulk (0.95 eV). The latter value is typical for ABO_3 perovskites (see *e.g.* experimental data ref. 17) whereas the reduced energy on the surface is also in line with the trend in our calculations for vacancies in $SrTiO_3$.[15,16]

We also simulated the process of the adsorbed O atom drop into the nearby vacancy (Fig. 4) and found an increase of the Mn–O binding energy by 0.74 eV but no energy barrier on the path of the adsorbed O atom penetration into a vacancy. Moreover, there is an additional energy gain of 2.83 eV when the adsorbed O atom penetrates the first surface plane.

Lastly, we studied the vertical adsorption of a free O_2 molecule in the pre-existing surface O vacancy. This is an energetically favourable process: for the final configuration shown in Fig. 3a the energy gain is 2.38 eV.

The key point here is that the energy barrier for O vacancy diffusion along the (001) surface is noticeably smaller than either the barrier for its diffusion in the bulk $LaMnO_3$, or the barrier for an adsorbed O atom migration. Therefore, the fast O atom transport at the cathode occurs due to diffusion of surface O vacancies. Since the barrier for the adsorbed O atom migration is high, these atoms are quite immobile and their penetration into the first plane of fuel cell cathode could occur predominantly upon their encounter with the mobile surface oxygen vacancies.

Surface stability under SOFC operation conditions

In order to analyze the relative stability of different $LaMnO_3$ surfaces under realistic operation conditions of the fuel cell, we performed an *ab initio* thermodynamic treatment, similar to that applied earlier to $BaZrO_3$[18] and $SrTiO_3$[19] surfaces. This method was developed following a general *ab initio* thermodynamic approach (ref. 20–25 and references therein). The most stable surface at any considered oxygen and manganese chemical potentials has the lowest surface Gibbs free energy. (Note that we do not consider vibrational entropy changes which are supposed to be small.[20])

We considered LaO- and MnO_2-terminated (001) surfaces built of *cubic* (high temperature) unit cells; $LaMnO_3$-, O_2-, and O-terminated (110) surfaces, and, finally, a MnO_2-terminated (001) surface with adsorbed O atom (hereafter MnO_2 + O-terminated surface). Since we assume the equilibrium of the surface with the bulk where the chemical potentials of three crystal constituents (La, Mn, and O) are interrelated by the condition $\mu(LaMnO_3) = \mu(La) + \mu(Mn) + 3\mu(O)$, only chemical potentials of two of these components are independent variables. Because oxygen atoms are in equilibrium on the surface and in the O_2 gas above the cathode surface and we have to account for a strong dependence of O chemical potential on the O_2 gas partial pressure and temperature, it is suitable to choose the O chemical potential as one of the independent variables in the surface Gibbs free energy whereas the Mn chemical potential can be taken as another independent variable. Following ref. 18 and 19 we calculate these quantities with respect to the energy per atom in Mn metal ($\Delta\mu$(Mn)) and O atom in a free O_2 molecule ($\Delta\mu$(O)).

We plotted the phase diagram on the l.h.s. of Fig. 5 which shows stability regions of different surfaces. The colour area here is limited at the bottom by the line where the chemical potential of La atoms in LMO becomes larger than in a metal, which corresponds to a La precipitation. On other sides, the coloured area is limited by lines, where the lowest surface Gibbs free energies become negative and the crystal spontaneously disintegrates. Only four different surfaces from the six considered could be stable: LaO-terminated (001) surface, MnO_2 + O-terminated (001) surface, O- and O_2- terminated (110) surfaces (the latter is not seen in Fig. 5 within the shown range of chemical potentials).

To determine the boundaries of the region where precipitation of La- and Mn oxides does not occur, we computed the *formation energies* (enthalpies) for related metal oxides. Results for the oxide formation energies are provided in Table 3 where calculations are also compared with experimental formation enthalpies. Our computations slightly overestimate the formation energies, which is commonly observed for the DFT with GGA functionals. Still, when we considered the formation of $LaMnO_3$ perovskite from the oxides with the same

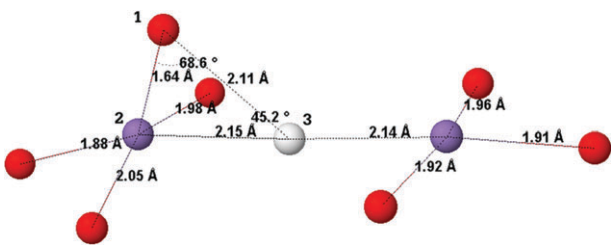

Fig. 4 Schematic view of the O atom 1 adsorbed atop the surface Mn_s atom 2 on the MnO_2-terminated surface dropping into an oxygen vacancy 3 on the orthorhombic (001) surface. The numbers are interatomic distances.

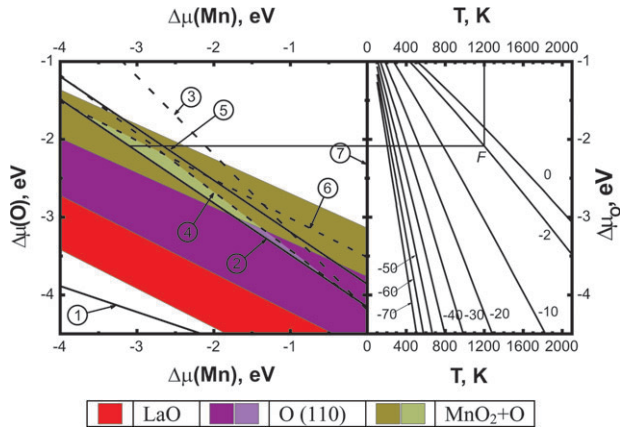

Fig. 5 Phase diagram: the regions of stability of $LaMnO_3$ surfaces with different terminations as functions of chemical potential variation for Mn and O atoms. The comparison includes LaMnO-, O_2-, and O-terminated (011) surfaces, LaO- and MnO_2- terminated (001) surfaces, and MnO_2-terminated (001) surface with an adsorbed O atom. The numbers in the circles point to the lines where metals or their oxides begin to precipitate: (1) metal La, (2) La_2O_3, (3) MnO_2, (4) Mn_3O_4, (5) Mn_2O_3, (6) MnO, and (7) metal Mn. The right side of the figures contains a family of $\Delta\mu_O$ as functions of the temperature at different oxygen gas pressures. The labels m on the oxygen lines indicate the gas pressure: 10^m atm.

oxidation states as in the perovskites, the obtained value matches very well that derived from experimental data.

The boundaries of the region where the $LaMnO_3$ crystal is stable with respect to decomposition into metals and their oxides, are represented in Fig. 5 by lines 1 to 7. Pure $LaMnO_3$ surfaces could exist only between these lines.[18,19] The stability region is limited by line 2 (precipitation of La_2O_3) on the bottom and by lines 4 and 6 (precipitation of Mn_3O_4 and MnO, respectively) on the top. This region is shaded in Fig. 5 with lighter colours. Because of the DFT shortcoming in the calculations of the relative energies for materials with a different degree of metal oxidation, one has to treat the obtained data with some caution. Therefore, we highlighted the lines of precipitation for 3-valent metal oxides La_2O_3 and Mn_2O_3 (solid lines 2 and 5), where the oxidation state is the same as in $LaMnO_3$. From all considered surfaces, only *two* turn out to be stable (within the region of $LaMnO_3$ crystal stability): (i) MnO_2-terminated (001) surface with adsorbed O atoms (MnO_2+O surface) at high O chemical potentials (O-rich limit) and low Mn chemical potential (Mn-poor limit) and (ii) O-terminated (110) surface at low O chemical potentials (O-poor limit) and high Mn chemical potential (Mn-reach limit). This result remains valid whether we include into consideration only precipitation of 3-valent La and Mn oxides or also an account for possible precipitation of all other manganese oxides.

On the r.h.s. of Fig. 5 we plotted the chemical potentials of the O atom derived from the experimental data (ref. 26). This window shows the dependence of the O chemical potential on temperature and O_2 partial pressure. Correct matching of the experimental curves with the computed stability diagram requires a correcting shift of the O atom chemical potential as explained in detail in ref. 18 and 19. We calculated the shift

Table 3 Calculated formation enthalpies ΔE_f (eV) for bulk oxides and $LaMnO_3$ perovskite. The second column contains experimental formation enthalpies for the oxides and $LaMnO_3$ ref. 26 at $T_0 = 298.15$ K, $p_0 = 1$ atm

Crystal	Calc. E_f/eV	Expt. ΔH_f/eV
La_2O_3	−18.86	−18.60
Mn_2O_3	−11.57	−9.92
MnO	−4.19	−3.99
MnO_2	−7.03	−5.39
Mn_3O_4	−16.70	−14.37
$LaMnO_3$	−15.66	−14.77
$LaMnO_3$ (from La_2O_3 and Mn_2O_3 oxides)	−0.498	−0.514

employing the same set of oxides used in this work and thus obtained an average shift of −0.77 eV value used in Fig. 5.

The combination of our surface stability diagram with the oxygen chemical potential as a function of temperature and O_2 partial pressure allows a detailed analysis of the trends under variable environmental conditions. Let us consider a situation typical for the fuel cell operation: $T \approx 1200$ K and oxygen partial pressure ranging between $p_{O_2} \approx 0.2$ and 0.01 atm (point *F* in Fig. 5). Our stability diagram demonstrates clearly that only the MnO_2-terminated (001) cubic surface with adsorbed O atoms is stable under the operational conditions (large O chemical potential, relatively high O pressure). The alternative (110) surface becomes dominant only at low O chemical potentials and thus very low oxygen pressures, $p_{O_2} \leq 10^{-10}$ atm.

Conclusions

Under the operational conditions of a fuel cell cathode, the cubic MnO_2 surface with adsorbed O atoms (with a considered coverage of 12.5%) is the most stable (in particular, more stable than (110) surfaces).

We have demonstrated that the $LaMnO_3$ (001) surface could be catalytically more active than isostructural $SrTiO_3$ since it permits dissociative O_2 adsorption on surface Mn ions even without the assistance of surface defects. The penetration of adsorbed O atoms into the first plane of cathode occurs very likely when it meets highly mobile surface O vacancies. The considerable difference of the oxygen vacancy formation energies on the surface and in the bulk (6.23 eV *vs* 7.64 eV) indicates their efficient segregation to the surface. The vacancy migration energy (0.67 eV) along the surface is smaller than in the bulk (0.95 eV) and enables fast surface diffusion of oxygen in the first cathode layer (rather than in the adsorbed state with the activation energy of 2 eV). We found no energy barrier for the last step of this process: a drop of O atom adsorbed atop the surface Mn ion into the nearby O vacancy. Direct incorporation of the O_2 molecule into an O vacancy is also energetically favourable.

We do not expect entropy effects to be large enough as to favour the diffusion in the adsorbed state over surface diffusion in the first layer; however it may seriously favour bulk diffusion at very high temperatures. Quantum MD simulations would be of great interest to clarify this point. A study of the influence of the electrolyte could be one of the next important steps.

Acknowledgements

The authors are greatly indebted to R. Merkle, D. Fuks, M. Liu, Y. Choi, J. Fleig, Yu. Zhukovskii, N. Kovaleva and H.-U. Habermeier for many stimulating discussions.

References

1. J. Fleig, K. D. Kreuer and J. Maier, in *Handbook of Advanced Ceramics*, Singapore, Elsevier, 2003, p. 57; J. Fleig, R. Merkle and J. Maier, *Phys. Chem. Chem. Phys.*, 2007, **9**, 2713.
2. R. Merkle and J. Maier, *Top. Catal.*, 2006, **38**, 141.
3. M. Bowen, M. Bibes, A. Barthélémy, J.-P. Contour, A. Anane, Y. Lemaître and A. Fert, *Appl. Phys. Lett.*, 2003, **82**, 233.
4. G. Banach and W. M. Temmerman, *Phys. Rev. B*, 2004, **69**, 054427; H. Zenia, G. A. Gehring, G. Banach and W. M. Temmerman, *Phys. Rev. B*, 2005, **71**, 024416.
5. R. A. Evarestov, E. A. Kotomin, Yu. A. Mastrikov, D. Gryaznov, E. Heifets and J. Maier, *Phys. Rev. B*, 2005, **72**, 214411; E. A. Kotomin, R. A. Evarestov, Yu. A. Mastrikov and J. Maier, *Phys. Chem. Chem. Phys.*, 2005, **7**, 2346–2350.
6. Y. Choi, D. S. Mebane, M. C. Lin and M. Liu, *Chem. Mater.*, 2007, **19**, 1690; Y. Choi, M. C. Lin and M. Liu, *Angew. Chem.*, 2007, **119**, 7352.
7. C. Noguera, *Physics and Chemistry of Oxide Surfaces*, Cambridge University Press, NY, 1996.
8. G. Kresse and J. Furthmueller, *VASP the Guide*, University of Vienna, Austria, 2003.
9. H. J. Monkhorst and J. D. Pack, *Phys. Rev. B*, 1976, **13**, 5188.
10. S. Piskunov, E. A. Kotomin, Yu. F. Zhukovskii, E. Heifets and D. E. Ellis, *Mater. Res. Soc. Symp. Proc.*, 2005, **894**, LL05–05.1.
11. G. Henkelman, A. Arnaldsson and H. Jónsson, *Comp. Mater. Sci.*, 2006, **36**, 354.
12. *CRC Handbook of Chemistry and Physics*, ed. D. R. Lide, CRC Press, Boca Raton, FL, 1993.
13. G. Henkelman, B. P. Uberuaga and H. Jónsson, *J. Chem. Phys.*, 2000, **113**, 9901.
14. G. Henkelman, G. Johannesson and H. Jónsson, in *Progress on Theoretical Chemistry and Physics*, ed. S. D. Schwartz, Kluwer, New York, 2000.
15. Yu. Zhukovskii, E. A. Kotomin, R. A. Evarestov and D. E. Ellis, *Int. J. Quantum Chem.*, 2007, **107**, 2956 (review article).
16. Denk, W. Munch and J. Maier, *J. Am. Ceram. Soc.*, 1995, **78**, 3265.
17. J. Carrasco, F. Illas, N. Lopez, E. A. Kotomin, Yu. F. Zhukovskii, R. A. Evarestov, Yu. A. Mastrikov, S. Piskunov and J. Maier, *Phys. Rev. B*, 2006, **73**, 064106.
18. E. Heifets, J. Ho and B. Merinov, *Phys. Rev. B*, 2007, **75**, 155431.
19. E. Heifets, S. Piskunov, E. A. Kotomin, Yu. F. Zhukovskii and D. E. Ellis, *Phys. Rev. B*, 2007, **75**, 115417.
20. K. Reuter and M. Scheffler, *Phys. Rev. B*, 2001, **65**, 035406.
21. K. Johnston, M. R. Castell, A. T. Paxton and M. W. Finnis, *Phys. Rev. B*, 2004, **70**, 085415.
22. J. Padilla and D. Vanderbilt, *Surf. Sci.*, 1998, **418**, 64.
23. F. Bottin, F. Finocchi and C. Noguera, *Phys. Rev. B*, 2003, **68**, 035418.
24. J. W. Cahn, in *Interfacial Segregation*, ed. W. C. Johnson and J. M. Blacely, American Society for Metals, Metals Park, Ohio, 1977, pp. 3–23.
25. I. Batyrev, A. Alavi and M. W. Finnis, *Faraday Discuss.*, 1999, **114**, 33.s
26. M. W. Chase, *NIST-JANAF Thermochemical Tables*, American Chemical Society, Washington, DC, 1998.